Journal of Raman Spectroscopy

WILEY

Journal of RAMAN SPECTROSCOPY

RESEARCH ARTICLE OPEN ACCESS

ECONOS 2024

Diagrammatic Schemes for Nonlinear Optical Interactions

F. Vergari[1,2] | F. Mazza[3] | A. Hosseinnia[3] | M. Marrocco[1]

[1]Dipartimento TERIN, ENEA, Rome, Italy | [2]Dipartimento di Fisica, Università di Roma "La Sapienza", Rome, Italy | [3]Faculty of Mechanical Engineering, RWTH Aachen University, Aachen, Germany

Correspondence: M. Marrocco (michele.marrocco@enea.it)

Received: 30 September 2024 | **Revised:** 23 January 2025 | **Accepted:** 2 February 2025

Keywords: diagrammatic perturbation theory | double-sided Feynman diagrams | Liouville space | nonlinear optics | Raman scattering

ABSTRACT

Nonlinear optical interactions are usually understood diagrammatically to sift only those contributions to the dielectric susceptibility that matter most to the signal being measured. Here, we review the main techniques of diagrammatic perturbation theory (i.e., double-sided Feynman diagrams, Liouville pathways, and Albrecht notation) that make use of the semiclassical approximation. A brief mention of other recent diagrammatic proposals is also made. The limitations of such approaches are discussed in view of a fully quantum-mechanical treatment of optical interactions. It is then suggested that the limitations of the conventional approaches can be overcome by a field-type modification of the Albrecht notation that combines the simplicity of the energy-level representation with the wealth of information provided by more elaborated diagrams (namely, double-sided Feynman diagrams and Liouville pathways). Rules to replace the Albrecht notation with the matter field representation are given, and instructive examples are illustrated for Raman spectroscopy.

1 | Introduction

The success of diagrams in physics comes from the power of images. In comparison with the analytic understanding of physics (i.e., exclusively based on math models), diagrams capture the essence of physical processes in a snapshot. One instructive example is the use of Feynman diagrams to speed up many difficult calculations of quantum field theory [1]. In close relation with this paradigmatic example, a variation of the Feynman diagrams has become popular in the application of perturbative methods to the calculation of any specific order of the density matrix whose elements solve the modified Liouville-von Neumann equation. The resulting diagrammatic approach takes advantage of the so-called double-sided Feynman diagrams (DSFDs) [2, 3]. The name comes from the graphic visualization of the two sides (i.e., bra and ket) of the density matrix in the perturbative regime. In addition to DSFDs, nonlinear optical interactions responsible for energy exchange between electromagnetic fields and molecules can be equally pictured by means of other diagrammatic techniques, namely, the method of Liouville pathways [2] and the energy ladder scheme, also known as Albrecht notation [4]. The former is an alternative diagrammatic approach where light–matter interaction creates pathways in a lattice made of all the possible combinations between bra and ket molecular states. The latter is an attempt at encoding the elaborate density matrix formalism into simpler energy ladder schemes.

In this paper, we briefly review the abovementioned techniques (note that we have no knowledge of existing reviews on the subject). After illustrating their use in avoiding cumbersome calculations, we highlight the main limitations of such techniques. We propose that the simplicity of energy ladder schemes can be extended to the description of optical interactions at the level of matter fields rather than of the energy they carry.

The work is organized as follows. First of all, in Section 2, the main diagrammatic techniques are reviewed in a fashion that is accessible to readers that are less familiar with diagrammatic

perturbation theory (DPT). Some recent suggestions of alternatives to conventional diagrams are also discussed in that section. After this preparatory material, Section 3 motivates our suggestion of the new diagrammatic scheme laid out in Section 4. Conclusions are in Section 5.

2 | Review of DPT

DPT of optical interactions is the outcome of several attempts made over decades of research on how to simplify the involved structure of the nonlinear dielectric susceptibility. To illustrate the difficulty in handling nonlinear optical interactions, it suffices to recall that the complete expression of the susceptibility up to the third order is made of tens of terms. For example, 48 terms cover the whole set of third-order contributions. Given this complexity, diagrammatic approaches are of assistance to sort out only those terms that are relevant to the specific interaction. Examples are given below.

The first suggestion of optical diagrams was made by Ward in 1965 who had the idea of adjusting the Feynman diagrams of quantum field theory to the physical constraints of molecular interactions [5]. The idea was based on the perturbative representation of the molecular state $|\psi>$

$$\left|\psi>\right. = \left(1 + GH' + GH'GH' + GH'GH'GH' + \ldots\right)\left|g>\right. \quad (1)$$

where $|g>$ is the ground state and G is the Green operator that propagates the state after the electric dipole interaction H'. In turn, the perturbative expansion of the polarization $P = <\psi|er|\psi>$ results from all the possible combinations of Equation (1) (i.e., the ket expansion) and its Hermitian conjugate $<\psi|$ (i.e., the bra expansion). For example, the case of second-harmonic generation (SHG) can be found thus after introducing the closure condition $\sum_n |n><n| = 1$ valid for the whole set of eigenstates $|n>$. The fundamental contribution $<g\left|H'G^{\dagger}\right|n'><n'|er|n><n|H'G|g>$ to the SHG polarization P can be diagrammatically sketched as shown in Figure 1. The horizontal line represents the evolution of the molecular state that, starting from the ground, goes back to it after the transitions $|g> \rightarrow |n>$, $|n> \rightarrow |n'>$, and $|n'> \rightarrow |g>$. Downward arrows specify the action of the perturbation. The upward arrow describes the final SHG polarization. Other nonlinear optical phenomena are diagrammatically represented in Ward [5], as well.

It took a while for Ward's idea to be acknowledged. However, some issues of his basic approach are immediately recognizable. The most evident shortcoming is the missing distinction

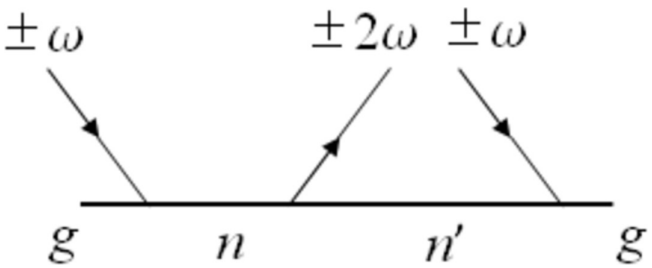

FIGURE 1 | Ward's representation of one diagrammatic contribution to the SHG susceptibility [5].

between bra and ket states. Furthermore, the final emission is not time ordered, and its either positive or negative sign is not linked to the arrow direction. These issues were solved by the slow adoption of the two-sided variant of the Feynman diagram (see Section 2.1), yet single-line diagrams survived for some time. The most evident example is reported in the celebrated book by Yariv [6]. Note that in the example of the two-photon process (see figure 3.2 in Yariv's text [6]), the energy scheme accompanies the Feynman diagram. The additional recourse to the energy scheme has become a common practice in DPT approaches, and nowadays, many publications report both diagrammatic representations. This suggests that a complete description of nonlinear optical processes requires the information provided by both energy diagrams and other diagrams drawn according to more sophisticated DPT techniques.

2.1 | DSFDs

The elegant suggestion of DSFDs came out in the wake of Ward's ideas. It was brought forth in 1976 by Bordé [7], and for this reason, DSFDs were initially recognized as Bordé diagrams [8]. Soon, different conventions concerning the rules for drawing DSFDs were formulated [9–15]. By the mid 80′, this diagrammatic technique was finally mature and acknowledged in nonlinear optics [16].

The key feature of DSFDs is that they reproduce the structure implied in the calculation of the density matrix, whose elements are $\rho_{nm} = <n|\hat{\rho}|m>$ with $\hat{\rho}$ the density operator [2, 3]. The elements satisfy the relaxed Liouville-von Neumann equation $i\hbar\dot{\rho}_{nm} = \left[\hat{H},\hat{\rho}\right]_{nm} - \gamma_{nm}\left(\rho_{nm} - \rho_{nm}^{eq}\right)$ that includes a phenomenological damping term. Given the structure of ρ_{nm}, bra and ket states undergo changes that are marked on a pair of Feynman diagrams drawn vertically. One vertical segment relates to the ket branch of the density matrix, whereas the other stands for the bra side. Time goes upward. Lines or arrows intersecting the diagram depict the fields. Points of intersections with the vertical bra and ket segments define events of light–matter interaction.

An example of DSFDs is shown in Figure 2. It portrays a contribution to stimulated Raman gain scattering (SRGS) via an R_3 response function (i.e., time-ordered bra/bra/ket interactions) and illustrates the four possible dipole interactions that are common to other possible time orderings.

More in detail, absorption is designated by means of an arrow pointing inward. Stimulated emission, much intuitively, is represented as an outward arrow. The arrows pointing to the right play the role of regular complex-valued fields. Those pointing to the left define the conjugate fields. Based on such simple rules, the first arrow appearing on the ket side of Figure 2 (third event on the time axis) describes the typical electric dipole coupling $\boldsymbol{\mu}_{ln} \cdot \boldsymbol{E}_q \, exp\left(i\boldsymbol{k}_q \cdot \boldsymbol{r} - i\omega_q t\right)$ between the dipole matrix element μ_{ln} and the electric field in the $\left(\boldsymbol{k}_q, \omega_q\right)$ mode. The other couplings contain, at least, one conjugate element (denoted by the asterisk). They are summarized as follows. The first interaction in time is again an absorption (incoming arrow on the bra side) whose coupling is $\boldsymbol{\mu}_{ln}^{*} \cdot \boldsymbol{E}_p^{*} \, exp\left(-i\boldsymbol{k}_p \cdot \boldsymbol{r} + i\omega_p t\right)$ between the conjugate of the dipole element $\boldsymbol{\mu}_{ln}$ and the conjugate of the field $\boldsymbol{E}_p \, exp\left(i\boldsymbol{k}_p \cdot \boldsymbol{r} - i\omega_p t\right)$ in the $\left(\boldsymbol{k}_p, \omega_p\right)$ mode. On the contrary, the

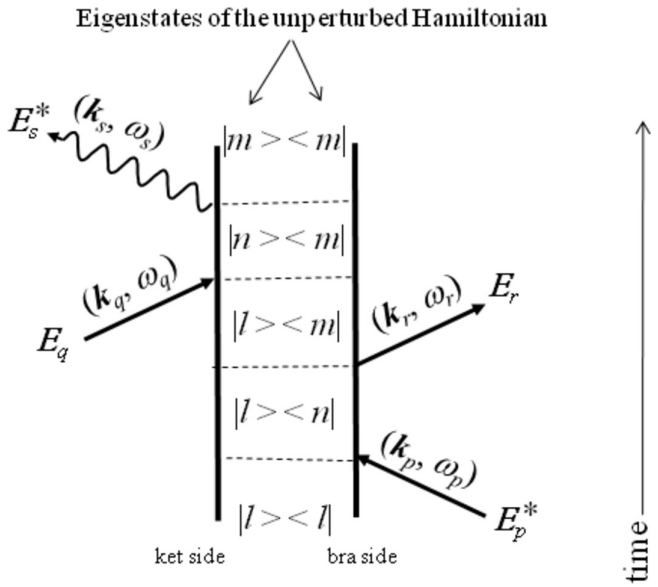

FIGURE 2 | An example of DSFD representing one possible contribution to stimulated Raman gain scattering.

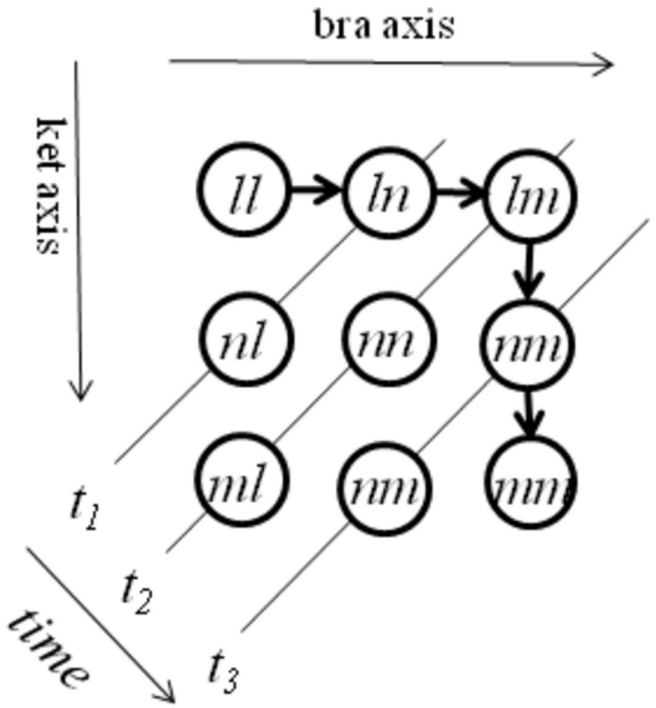

FIGURE 3 | Liouville space coupling scheme for third-order nonlinear interactions. The represented pathway (ordered bold arrows) corresponds to the DSFD of Figure 2.

second interaction on the time axis is an emission on the bra side and determines the coupling $\boldsymbol{\mu}_{nm}^* \cdot \boldsymbol{E}_r \, exp(i\boldsymbol{k}_r \cdot \boldsymbol{r} - i\omega_r t)$. The final emission gives a contribution to the total scattered signal and arises from the coupling $\boldsymbol{\mu}_{nm} \cdot \boldsymbol{E}_s^* \, exp(-ik_s \cdot r + i\omega_s t)$ on the ket side. Given the relevant role of the scattered signal in the actual optical measurement, a wavy line is chosen to remark the final emission. Note that, between two consecutive interactions, the molecule evolves freely under the effect of the unperturbed Hamiltonian.

Following the rules outlined above, we can write an explicit formula to compute the susceptibility. To do so, some further criteria are, however, needed. Importantly, they allow for the translation of the graphic language into the correct math. Such criteria lie outside the scope of this review and are not discussed further here but can be found elsewhere [2, 3, 8, 16].

2.2 | Liouville Pathways

The designation of Liouville space is credited to Fano who used it in treating pressure broadening [17]. Twenty years later, Mukamel introduced it in the diagrammatic theory of four-wave mixing [18].

The vectorial structure of the Liouville space comes from its basis vectors $|n><m|$ representing the fundamental structure on which the density operator is defined ($\hat{\rho} = \rho_{nm}|n><m|$, summation over repeated indices). A linear combination of such elements gives the ket vector $|\rho\gg$ (double curly bracket intended), whereas the bra vector $\ll\rho| = (|\rho\gg)^\dagger$ is obtained via ordinary Hermitian conjugation. Additional properties of the Liouville space are summarized in Mukamel [2]. Nonetheless, even within the limited scope of this brief summary, it is intuitive to construct the Liouville space by means of the Liouville basis $|n><m|$.

The coupling scheme, connecting the basis vectors and their duals, forms a two-dimensional lattice whose points are joined via arrows that symbolize dipole interactions. Figure 3 provides an example that refers to the same physical process described by the DSFD of Figure 2.

The rules for the construction of the Liouville space coupling scheme can be easily generalized beyond the specific example provided in Figure 3. The first step is to consider the initial element $|l><l|$ on the top-left corner of the lattice ($|\rho(t \to -\infty)\gg = |l><l|$). This element marks the starting point of several pathways that can be obtained after state evolution along the bra and ket branches of the density matrix. Thus, any change in the branches generates a motion within the lattice of the coupling scheme whose horizontal and vertical axes define the directions of the bra and ket dynamics (each axis can be arbitrarily chosen to represent the motion for one vector type or the other).

The specific pathway highlighted in Figure 3 is easily understood as follows. The first interaction on the bra side entails the horizontal motion $|l><l| \to |l><n|$ at time t_1. The alternative downward motion $|l><l| \to |n><l|$, which is not part of the pathway considered here, would give rise to a different contribution to the susceptibility (i.e., R_4 form of the response function with time-ordered ket/bra/bra interactions). This implies that the time direction agrees with the left-to-right motion along the diagonal of the square lattice of Figure 3. In other words, the possible ket evolution, an alternative to the bra motion considered in Figure 3, would take place at the same time t_1. Analogous choices between ket and bra paths are available at each time step, and additional pathways can be added to the isolated pathway sketched in Figure 3 (bold arrows).

Clearly, more rules are necessary to convert the coupling scheme into the mathematical expression of the susceptibility. They are

available elsewhere [2, 18], and their outline is not within the scope of the present summary, where we focus on the diagrammatic features of DPT approaches.

2.3 | Albrecht Notation

A third DPT technique was developed in 1985 by Lee and Albrecht [4]. It bears the name of the second author who disseminated the workings of the technique in several later publications.

The rationale behind the Albrecht notation is that energy-level diagrams are very intuitive. States of higher or lower energies are more neatly distinguished in energy schemes than in DSFD diagrams and Liouville pathways. Clearly, the description based on an energy scheme encounters the obvious difficulty that the interactions happen at the level of matter states where the distinction between bra and ket vectors do matter. This piece of information is lost in energy schemes. This limitation, analog to the one caused by the missing information on bra and ket events in ordinary (i.e., single-sided) Feynman diagrams, can be overcome with the help of different graphic notations for those field lines of the energy ladder that act on either the bra or the ket sides of the density matrix. The rules can be recapitulated with the guide of Figure 4. It displays the Albrecht notation for the same nonlinear interactions of Figures 2 and 3. In this way, the reader can weigh the pros and cons of the three techniques.

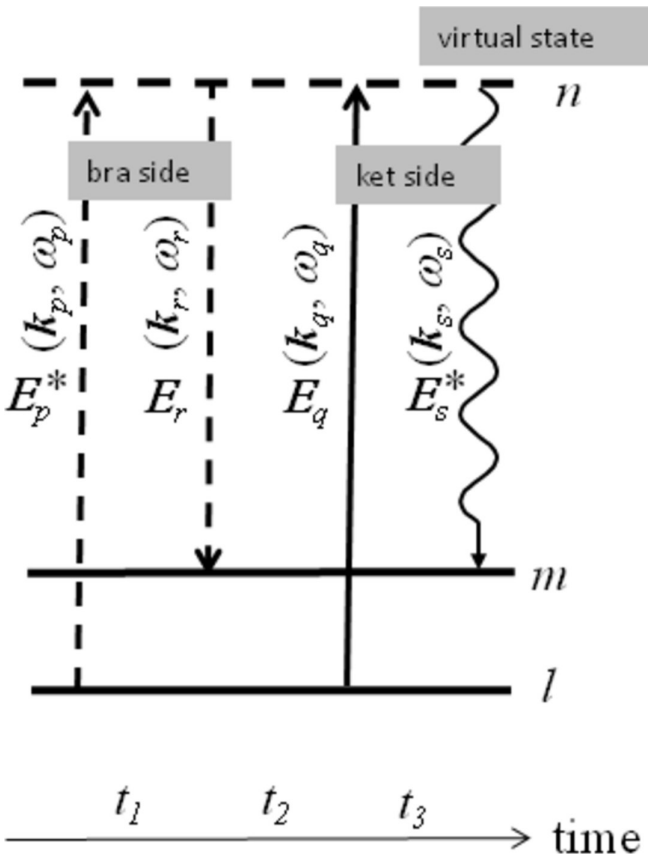

FIGURE 4 | Albrecht notation for the nonlinear optical process described by the diagrams of Figures 2 and 3.

Fields acting on the bra side are depicted by means of broken lines. Conventional solid lines are instead drawn for fields acting on the ket side. The final emission is a wavy solid line to remark the contribution to the detected signal. Time propagates to the right. Note that the energy levels have been labeled by letters that hint to, but do not correspond with, the quantum mechanical states (e.g., n in place of $|n>$). The difference underlines the fact that a state provides a field-type information, and consequently, energy ladder schemes with ket state labels are misleading.

The simplicity inherent in the Albrecht notation makes the corresponding diagrammatic scheme a popular choice in technical literature, as evidenced by some examples of our choice [19–21]. This same straightforwardness serves as a guiding principle for our proposal of a novel DPT technique, the details of which are explored in Section 4.

2.4 | Further Research

The three major DPT techniques presented above are not exhaustive of the diagrammatic tools used to study optical interactions. Minor alternatives are known. We briefly discuss some of them below.

Classical diagrammatic analogs to DSFDs have been introduced to describe a classical anharmonic oscillator undergoing third-order interactions [22]. The classical diagrams are nothing else than polylines of (classical) field wavevectors taken with their own signs. A positive sign determines a positive slope in the chain. A negative sign means a negative slope. This simple rule generates six polylines. The number is not a coincidence. Six are, indeed, the available permutations of the three wavevectors. Thereafter, each polyline is shown to be equivalent, in the classical limit ($\hbar \to 0$), to a set of eight DSFDs. The whole set of six polylines amounts to the 48 DSFDs expected for the contributions to the third-order susceptibility.

Another form of Feynman diagrams has been suggested for composite systems made of more than one interacting object (for instance, substrate-molecule interface) [23]. These diagrams can be regarded as a restoration of single-line Feynman diagrams, but they differ in their circular shape. Each circle relates to only one of the quantum-mechanical objects that make up the composite system. Highlighted points on each circular loop are those where the interactions take place following the clockwise evolution of the ket state. Virtual bosons (i.e., not exclusively photons) are interaction carriers within the composite system and are visualized as broken lines. These connect different loops. Thus, the number of connections corresponds to the number of virtual bosons exchanged between loops, and the diagrams can be organized hierarchically, depending on the number of virtual bosons. The new technique has been applied so far to sum-frequency generation [23].

A fundamental boundary of ordinary nonlinear optics is its QED generalization where fields are no longer classical objects. As a matter of fact, the semiclassical approximation was tacitly

assumed in summarizing the three main DPT techniques. When the approximation does not hold, fields are necessarily treated as operators and various authors have contributed different answers to the question of how the diagrams should be modified in the QED picture. A brief account of their proposals is given below.

A DSFD variant is introduced in Marx et al. [24] and further explained in Mukamel and Rahav [25]. It is referred to as closed-time-path-loop (CPTL) diagrams. Differently from the more conventional DSFDs, CTPL drawings do not entirely follow the temporal sequence of the interactions. They are only partially time ordered to the extent that time flows vertically upward on the ket side (forward direction) and then turns downward on the bra side (backward direction). The shift implies that time ordering is, however, obeyed in each branch. This modification appears to be useful for frequency-dependent calculations (typical in QED applications) where the sequence of interactions is hidden in the frequency domain. Understandably, fewer CPTL diagrams are required to recap the information resulting from the sum of several DSFDs accounting for all the possible time orderings on the bra and ket branches.

To conclude this section, we consider another diagrammatic approach meant for a fully quantum description of nonlinear optics [26]. The approach relies on a state sequence based on the number of photons rather than on the molecular states. This criterion dictates that the initial photonic state is defined according to the number of incoming photons (for instance, 2 at a given frequency suitable for SHG) whereas the final state is defined according to the outgoing photons (for SHG, zero photons at the original frequency and one photon at twice the original frequency). In between, interactions are expected to alter the number of photons, and each possible change is coupled to a molecular state. This technique is claimed to be effective in simplifying cooperative phenomena where two or more molecules (or other quantum particles, such as nanoparticles) are coupled by means of laser beams.

3 | Motivations for an Alternative Representation

Some of the recent diagrammatic techniques briefly discussed in Sect. 2.4 have underlined the necessity of modifying the conventional DPT approaches to make them more suitable for the fully quantum-mechanical treatment of optical interactions [24–26]. The interest in the QED formalism of nonlinear optics is especially propelled by the emerging field of topological photonics [27]. In addition, purely spectroscopic reasons suggest the use of QED tools. One relevant example is provided by cascading processes where excited molecules generate secondary fields that interact with other molecules and mix with the primary exciting fields [28]. Given the interest in QED applications, we introduce next a new variant of conventional DSFDs that better agrees with a fully quantum-mechanical description. Before describing our suggestion in detail, we would like to underscore some additional issues with DPT that motivate our work.

Canonical diagrammatic representations have additional limitations. The most obvious emerges in the description of optical processes when the number of photons is low and the QED machinery is mandatory for a correct interpretation [29]. As a matter of fact, absorption and stimulated emission are regarded, within the semiclassical approach, as caused by so many photons that the fields are conventionally classical. When this circumstance does not hold, we might wonder how to properly modify the corresponding diagrams.

One of the many examples of this issue is provided by the DSFD for spontaneous Raman scattering (SpRS). The quantum theory dictates that an apparently linear process within the classical approach (oscillating dipole) becomes a $\chi^{(3)}$ process owing to the action of the vacuum field [30]. Its diagrammatic analysis is shown in Figure 5. Besides the ordinary interaction with the strong field in the $(\boldsymbol{k}_1, \omega_1)$ mode, the coupling with the vacuum field in the $(\boldsymbol{k}_2, \omega_2)$ introduces the additional interactions that make both diagrams of Figure 5 look like those of the semiclassical representations of stimulated Raman scattering in Figures 3 and 4.

The main difference comes from the quantum-mechanical representation of the fields [29]. Their classical amplitudes E and E^* are now replaced by the annihilation and creation operators a and $a^\dagger$ (bosonic ladder operators). In this respect, the most appropriate QED framework is the second quantization of the molecular Hamiltonian whose electric-dipole term entails the couplings $\pi^\dagger a$ and $a^\dagger \pi$, where π and $\pi^\dagger$ are the molecular transition operators [29]. If the electric-dipole coupling is g_{ED}, which

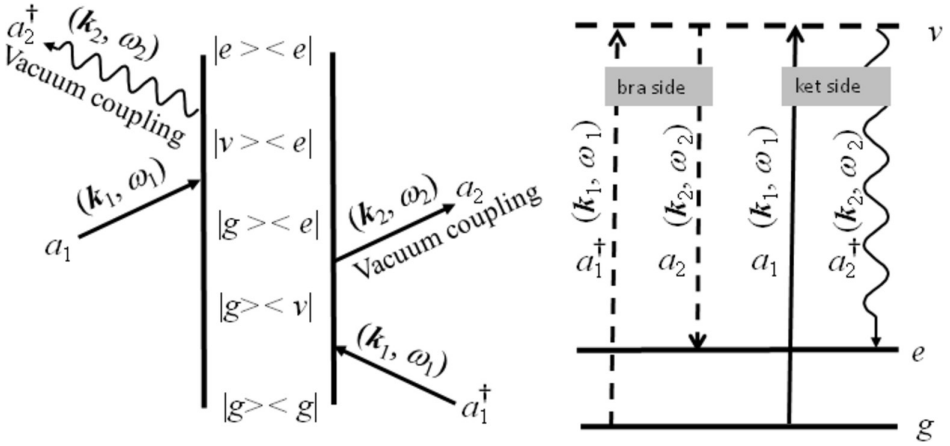

FIGURE 5 | DSFD and Albrecht diagram representing the quantum description of SpRS.

is a real quantity with units of frequency, the electric-dipole interaction is

$$H_{ED} = i\hbar g_{ED}\left[\pi^{\dagger} a\, exp(i\boldsymbol{k}\cdot\boldsymbol{r}) - a^{\dagger}\pi\, exp(-i\boldsymbol{k}\cdot\boldsymbol{r})\right]. \quad (2)$$

In particular, considering the example in Figure 5, the first interaction on the bra side happens under the effect of $< g, n_1, 0_2 \mid \pi_{gv} a_1^{+} \rightarrow < v, n_1 - 1, 0_2 \mid$ where the notation refers to the initial combined state of the molecule-radiation system with n_1 photons in the $(\boldsymbol{k}_1, \omega_1)$ mode and the quantum vacuum in the $(\boldsymbol{k}_2, \omega_2)$ mode. The second interaction happens under the effect of $< v, n_1 - 1, 0_2 \mid \pi_{ve}^{+} a_2 \rightarrow < e, n_1 - 1, 1_2 \mid$ where one-photon bra state is now present in the second mode. As a result, the absorption of the strong field is described by means of the creation operator a_1^{+}. Conversely, the vacuum coupling that gives rise to the bra emission is through the annihilation operator a_2 of the second mode. Thus, the action of the radiation field seems in contradiction with the notation used for both diagrams in Figure 5 (creation operator for an absorption and destruction operator for an emission). The conclusion is that the notation for the bra side in conventional DSFDs is rather bizarre.

The oddity arising in the fully quantum description adds to the redundancy of information when DSFDs and energy ladder schemes are employed together [21, 31–34]. This motivates us in looking for a novel DPT technique.

4 | Matter Field Representation (MFR)

Among the major DPT approaches, the energy ladder is the most intuitive and easy to read. For this reason, we focus on this type of representation.

As discussed in Section 2.3, the main problem is that the energy levels conceal the detailed information about the interactions involving bra and ket states. Indeed, in many simplistic descriptions of nonlinear optical processes, the energy levels are reported without consideration for the details of the interactions. Representing these details in the DPT picture requires the field information to be included in the energy ladder scheme. To achieve this, we turn the Albrecht notation into a MFR.

We begin by recalling that ket and bra vectors are Hermitian conjugate of each other, have unitary norm ($< n \mid n > = 1$), and define the energy spectrum ($\epsilon_n = < n\left|\hat{H}_0\right|n >$) of the unperturbed Hamiltonian $\hat{H}_0$ that is supposed dimensionless. Importantly for our argument, the conjugation corresponds to a reflection about the real axis of the complex plane. This one is designed to accommodate ket vectors defined as $\mid \eta > = \epsilon_n \mid n >$. The rescaling leads to $\epsilon_n^2 = < \eta \mid \eta >$. Finally, the correspondence $\mid n > \rightarrow z_n = \mid \eta >$ generates the bra vector $< \eta \mid$ after the reflection of z_n about the real axis. Clearly, the inverse procedure would generate the ket vector $z_n = \mid \eta >$ if we started by considering the bra vector $< \eta \mid$.

The objective of this simple procedure is to get a dilation (or a contraction) of the complex plane where the original ket and bra vectors live. In this way, the length of the rescaled vectors quantifies the corresponding energy levels.

The procedure is applied to the energy levels shown in the left panel of Figure 6. We can focus on two energy levels: ϵ_a and ϵ_b. The scaling of the ket vectors $\mid a >$ and $\mid b >$ leads to the new vectors (here represented by complex-valued numbers) $z_a = \epsilon_a \mid a >$ and $z_b = \epsilon_b \mid b >$. These are, by definition, found in the upper half of the complex plane. The phases φ_a and φ_b are arbitrarily determined without loss of generality and the lengths ϵ_a of z_a and ϵ_b of z_b are reported on the imaginary axis. These values are projected to the right in order to define the vertical scale where to place the diagrammatic representation of the ket states. After reflections of z_a and z_b about the real axis, the bra states can be eventually located in the MFR diagram (right panel of Figure 6). Note that the linearity of the vertical scale of the diagram is irrelevant to the graphic purposes. A final comment regards the lowest energy level ϵ_r. Since this level provides the reference of the relative energy, its null radius entails a degenerate MFR level where $\mid r >$ and $< r \mid$ are located (thicker line in the right panel of Figure 6). It is often the case that such a level coincides with the ground state vectors. However, in general, it might happen that the reference is taken at a different state.

This example illustrates the desired changes to the usual energy level scheme. Taking again the case of SpRS in Figure 5, the corresponding MFR diagram is in Figure 7. Besides the

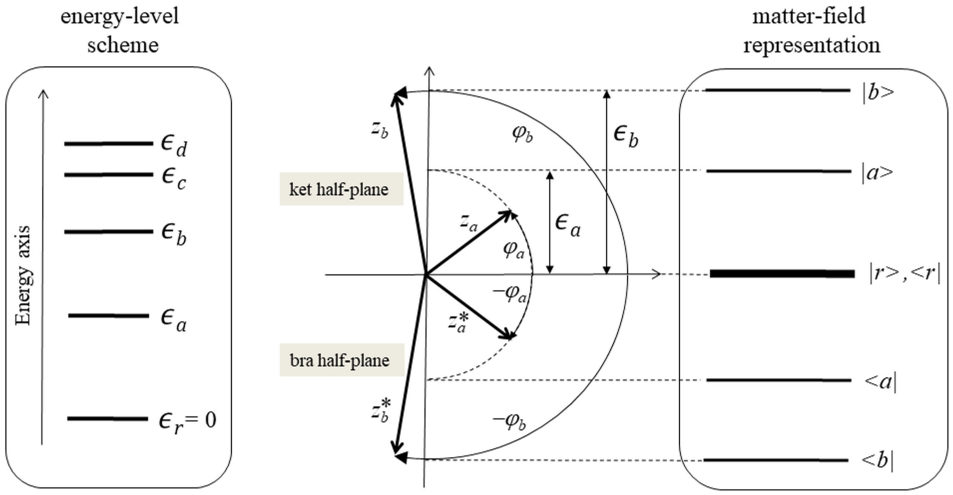

FIGURE 6 | Left: usual energy scheme. Right: matter field representation of energy levels.

appearance of the bra states underneath the ket states, the main difference with respect to the usual Albrecht notation is that now the interactions involving the bra branch agree with the action of the ladder operators of the dipole interaction (i.e. annihilation for absorption, creation for emission). Given this agreement, the broken lines used for bra dipole interactions in the Albrecht notation are no longer necessary and are thus replaced by solid lines.

We can furthermore comment on the extension of MFR to the semiclassical approach. There is actually no formal impediment to this. Let us consider the DSFD in Figure 2, the inward arrow on the left and the outward on the right represent classical fields with amplitudes $\boldsymbol{E}_q$ and $\boldsymbol{E}_r$. However, both of them would represent the action of the corresponding annihilation operators if the fields were quantized and are thus represented as up-going arrows in MFR diagrams. Similarly, the common direction of the arrows representing the classical fields of amplitudes $\boldsymbol{E}_p^*$ and $\boldsymbol{E}_s^*$ in the DSFD in Figure 2 suggests a common action of the corresponding creation operators visualized as downward arrows in the MFR diagram in Figure 7. This is not surprising given the ordinary replacement in QED of classical electric fields and their conjugates with annihilation and creation operators.

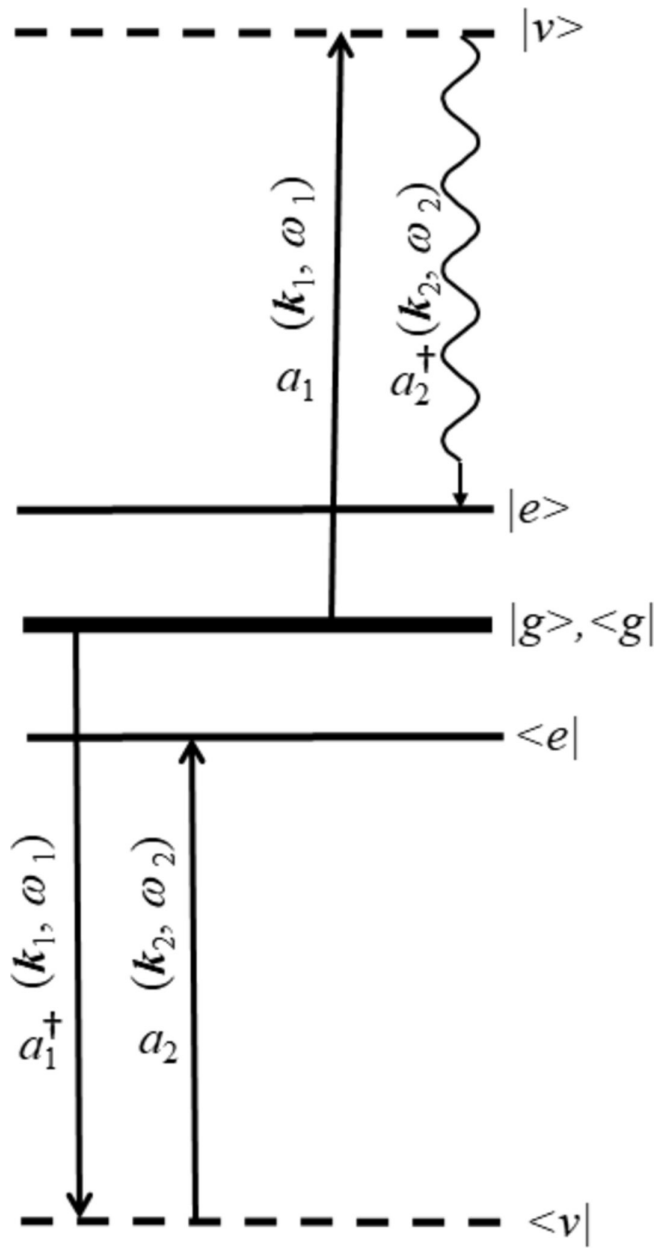

FIGURE 7 | Matter field representation of the Albrecht diagram in Figure 5.

To conclude the present work, we highlight differences and connections between the traditional diagrammatic approaches and the present proposal. Let us consider one of the possible contributions to coherent anti-Stokes Raman scattering (CARS). We refer to the DSFD number 38 in Prior [14] and reproduced in Figure 8a.

The peculiarity of this CARS contribution is its presence even if the three laser pulses are delayed with respect to each other. Clearly, the resonance at the excited levels has the effect of generating a susceptibility term of minor importance in comparison with the strongest term with exclusively ket interactions that feature a resonance at the lowest levels. On the other hand, the contribution reported in Figure 8 presents a good mix of bra and ket as well as absorption and emission, which makes it an instructive example for comparison. In addition, the contribution has been the subject of different studies [35–37] and is worth discussing.

As anticipated in Section 2, the DSFD and the Liouville scheme are equivalently informative of the evolution of the bra and ket states. The two diagrams are shown in Figure 8a,b, respectively. However, other important pieces of information are missing. For example, by looking at those two diagrams only, one could not tell that this CARS contribution does not involve any virtual state. More importantly, we cannot extract the information about which frequency of the fields is the greatest or the smallest (equivalently, for the energy levels). These limitations are solved in the Albrecht diagram of Figure 8c where a hypothetical virtual state would be clearly denoted by a dashed line, as seen in Figure 4 (note that a final virtual level below the initial state appears in the Albrecht diagram reported elsewhere [35, 36] for the process considered in Figure 8c). The problem with the energy-level scheme is, however, the representation of the bra interactions. The bra arrows are, indeed, misleading. Absorption means an actual emission and vice versa. The DSFD shares the same contradiction, whereas the distinction between emission and absorption is even less clear in the Liouville pathway. In the MFR diagram of Figure 8d (not in scale with Figure 8c to save space in the whole figure), the information about ket and bra dynamics is well distinguished thanks to the separation between the two half-planes. Thus, the composition $|\,ket > < bra\,|$ typical of Figure 8a,b can be obtained at each time instant by taking note of the two level states reached by the most recent interactions (arrows) in the two respective half-planes (for instance, $|\,e' > < e\,|$ during the time frame between the two arrows in the bra half-plane). Furthermore, the agreement between the graphic symbol and the corresponding coherent process of absorption or emission is guaranteed. In the end, Figure 8d seems to condense the most complete knowledge about the optical interactions contributing to the build-up of the susceptibility.

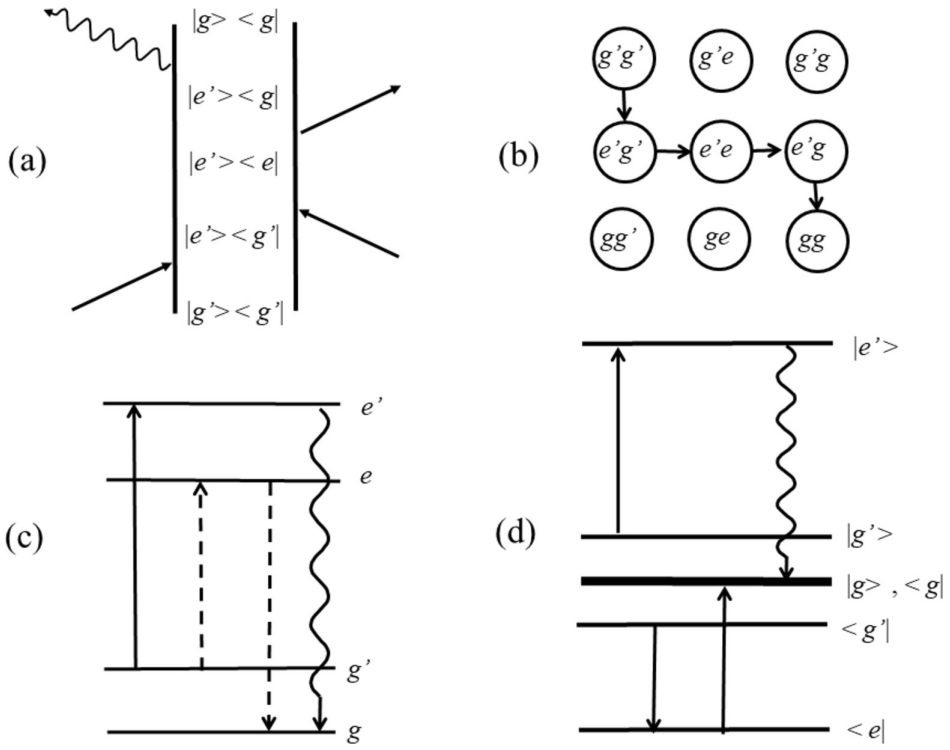

FIGURE 8 | Comparison of the three main diagrammatic techniques and the MFR proposed here. The diagrams refer to one minor contribution to CARS.

5 | Conclusions

To conclude, this work reports on the DPT of nonlinear optics with particular regard to Raman interactions.

In the first part, a review of the main DPT approaches is presented for the first time. Three conventional diagrammatic schemes are most commonly employed. One is rather popular (double-sided Feynman diagrams). The other two (Liouville pathways and Albrecht notation), although less popular, appear in many studies. The basic pictorial grammar of each technique is explained without paying attention to the rules that guide the translation into math language. Furthermore, a brief introduction to some recent DPT alternatives is also given.

In the second part, motivations for a new DPT approach are outlined. The main point of concern is about the ambiguity in the conventional diagrammatic representations of events on the bra side of the density matrix when the interacting fields are quantized (i.e., photon absorption being represented by a creation operator and stimulated emission by an annihilation operator). To resolve this, we introduced a modification of the Albrecht notation. The change is justified by a simple argument revolving around the renormalization of the molecular states to their energies. This paves the way for a graphic version of the energy levels in terms of their rescaled bra and ket vectors on a complex plane. The projections of their amplitudes in a time sequence complete the transformation of the energy-level diagram into its MFR. Owing to this simple manipulation, the ambiguity between bra absorption/emission and bosonic ladder operators disappears. Furthermore, the simplicity of energy ladder schemes and the rich field-type information provided by more sophisticated diagrammatic approaches are seamlessly combined in one diagram. The MFR thus overcomes the need for employing a couple of conventional diagrammatic representations (typically, Feynman diagrams plus energy-level schemes) found elsewhere. The extension of the MFR to the semiclassical DPT is also remarked.

Conflicts of Interest

The authors declare no conflicts of interest.

References

1. M. E. Peskin and D. V. Schroeder, *An Introduction to Quantum Field Theory* (New York: Addison-Wesley, 1995).

2. S. Mukamel, *Principles of Nonlinear Optical Spectroscopy* (Oxford: Oxford University Press, 1995).

3. R. W. Boyd, *Nonlinear Optics* (New York: Academic Press, 2008).

4. D. Lee and A. C. Albrecht, *Advances Infrared and Raman Spectroscopy*, eds. R. J. Clark and R. E. Hester (London: John Wiley & Sons, 1985): 179–213.

5. J. F. Ward, "Calculation of Nonlinear Optical Susceptibilities Using Diagrammatic Perturbation Theory," *Reviews of Modern Physics* 37 (1965): 1–18.

6. A. Yariv, *Quantum Electronics* (New York: John Wiley & Sons, 1989).

7. C. J. Bordé, "Forme de raie en spectroscopie à deux quanta sans élargissement Doppler," *Comptes Rendus de l'Académie des Sciences (Paris)* 282B (1976): 341.

8. M. D. Levenson, *Introduction to Nonlinear Laser Spectroscopy* (New York: Academic Press, 1982) INTRODUCTION.

9. T. K. Yee, T. K. Gustafson, S. A. J. Druet, and J.-P. E. Taran, "Diagrammatic Evaluation of the Density Operator for Nonlinear Optical Calculations," *Optics Communication* 23, no. 1 (1977): 7.

10. T. K. Yee and T. K. Gustafson, "Diagrammatic Analysis of the Density Operator for Nonlinear Optical Calculations: Pulsed and CW Responses," *Physical Review A* 18 (1978): 1597–1617.

11. J. Bordé and C. J. Bordé, "Intensities of Hyperfine Components in Saturation Spectroscopy," *Journal of Molecular Spectroscopy* 78 (1979): 353–378.

12. S. A. J. Druet and J. P. E. Taran, "Cars Spectroscopy," *Progress in Quantum Electronics* 7, no. 1 (1981): 72.

13. J. G. Fujimoto and T. K. Yee, "Diagrammatic Analysis of Third Order Nonlinear Optical Processes," *IEEE Journal of Quantum Electronics* 19 (1983): 861–872.

14. Y. Prior, "A Complete Expression for the Third-Order Susceptibility ($\chi(3)$)—Perturbative and Diagrammatic Approaches," *IEEE Journal of Quantum Electronics* 20 (1984): 37–42.

15. R. W. Boyd and S. Mukamel, "Origin of Spectral Holes in Pump-Probe Studies of Homogeneously Broadened Lines," *Physical Review A* 29 (1984): 1973–1983.

16. Y. R. Shen, *The Principles of Nonlinear Optics* (New York: Wiley, 1984).

17. U. Fano, "Pressure Broadening as a Prototype of Relaxation," *Physics Review* 131 (1963): 259–268.

18. S. Mukamel, "Nonimpact Unified Theory of Four-Wave Mixing and Two-Photon Processes," *Physical Review A* 28 (1983): 3480–3492.

19. B. Dunlap, K. C. Wilson, and D. W. McCamant, "Phase-Matching and Dilution Effects in Two-Dimensional Femtosecond Stimulated Raman Spectroscopy," *Journal of Physical Chemistry. A* 117 (2013): 6205–6216.

20. G. Batignani, C. Ferrante, and T. Scopigno, "Accessing Excited State Molecular Vibrations by Femtosecond Stimulated Raman Spectroscopy," *Journal of Physical Chemistry Letters* 11 (2020): 7805–7813.

21. A. L. Dobryakov, O. A. Krohn, M. Quick, I. N. Ioffe, and S. A. Novalenko, "Positive and Negative Signal and Line Shape in Stimulated Raman Spectroscopy: Resonance Femtosecond Raman Spectra of Diphenylbutadiene," *Journal of Chemical Physics* 156 (2022): 084304.

22. W. G. Noid and R. F. Loring, "Interpreting Nonlinear Vibrational Spectroscopy With the Classical Mechanical Analogs of Double-Sided Feynman Diagrams," *Journal of Chemical Physics* 121 (2004): 7057–7069.

23. T. Noblet, B. Busson, and C. Humbert, "Diagrammatic Theory of Linear and Nonlinear Optics for Composite Systems," *Physical Review A* 104 (2021): 063504.

24. C. A. Marx, U. Harbola, and S. Mukamel, "Nonlinear Optical Spectroscopy of Single, Few, and Many Molecules: Nonequilibrium Green's Function QED Approach," *Physical Review A* 77 (2008): 022110.

25. S. Mukamel, S. Rahav, "Ultrafast Nonlinear Optical Signals Viewed From the Molecule's Perspective," *Advances in Atomic, Molecular, and Optical Physics*, vol. 59, 223 (Elsevier, 2010).

26. D. L. Andrews, D. S. Bradshaw, K. A. Forbes, and A. Salam, "Quantum Electrodynamics in Modern Optics and Photonics: Tutorial," *Journal of the Optical Society of America B: Optical Physics* 37 (2020): 1153.

27. T. Ozawa, H. M. Price, A. Amo, et al., "Topological photonics," *Reviews of Modern Physics* 91 (2019): 015006.

28. K. Bennet, V. Y. Chernyak, and S. Mukamel, "Discriminating Cascading Processes in Nonlinear Optics: A QED Analysis Based on Their Molecular and Geometric Origin," *Physical Review A* 95 (2017): 033840.

29. R. Loudon, *The Quantum Theory of Light* (Oxford: Oxford University Press, 2000).

30. E. O. Potma and S. Mukamel, *Coherent Raman Scattering Microscopy*, eds. J.-X. Chen and X. S. Xie (Boca Raton: CRC Press, 2012): 3–35.

31. K. Okumura and Y. Tanimura, "Energy-Level Diagrams and Their Contribution to Fifth-Order Raman and Second-Order Infrared Responses: Distinction Between Relaxation Models by Two-Dimensional Spectroscopy," *Journal of Physical Chemistry. A* 107 (2003): 8092–8105.

32. X. Qiu, X. Li, K. Niu, and S.-Y. Lee, "Inverse Raman Bands in Ultrafast Raman Loss Spectroscopy," *Journal of Chemical Physics* 135 (2011): 164502.

33. K. Niu and S.-Y. Lee, "Analysis of Time Resolved Femtosecond and Femtosecond/Picosecond Coherent Anti-Stokes Raman Spectroscopy: Application to Toluene and Rhodamine 6G," *Journal of Chemical Physics* 136 (2012): 064504.

34. N. Fukutake, "Comparison of Image-Formation Properties of Coherent Nonlinear Microscopy by Means of Double-Sided Feynman Diagrams," *Journal of the Optical Society of America B: Optical Physics* 30 (2013): 2665.

35. T. Chen, V. Engel, M. Heid, et al., "Determination of Wave Packet Dynamics by Femtosecond Time-Resolved Pump-Dump-Probe and Four-Wave Mixing Techniques," *Journal of Molecular Structure* 480-481 (1999): 33–43.

36. J. Faeder, I. Pinkas, G. Knopp, Y. Pior, and D. J. Tannor, "Vibrational Polarization Beats in Femtosecond Coherent Anti-Stokes Raman Spectroscopy: A Signature of Dissociative Pump–Dump–Pump Wave Packet Dynamics," *Journal of Chemical Physics* 115 (2001): 8440–8454.

37. R. Lausten, O. Smirnova, B. J. Sussman, S. Gräfe, A. S. Mouritzen, and A. Stolow, "Time- and Frequency-Resolved Coherent Anti-Stokes Raman Scattering Spectroscopy With Sub-25fs Laser Pulses," *Journal of Chemical Physics* 128 (2008): 244310.